# Crystal structure of an empty capsid of turnip yellow mosaic virus

Roon, A.M.M. van; Bink, H.H.J.; Plaisier, J.R.; Pleij, C.W.A.; Abrahams, J.P.; Pannu, N.S.

doi:10.1016/j.jmb.2004.06.085 J. Mol. Biol. (2004) 341, 1205–1214

JMB

Available online at www.sciencedirect.com

SCIENCE DIRECT®

ELSEVIER

# Crystal Structure of an Empty Capsid of Turnip Yellow Mosaic Virus

**Anne-Marie M. van Roon[1], Hugo H. J. Bink[2], Jasper R. Plaisier[1] Cornelis W. A. Pleij[2], Jan Pieter Abrahams[1] and Navraj S. Pannu[1]***

[1]*Biophysical Structural Chemistry, Leiden Institute of Chemistry, P.O. Box 9502 2300 RA Leiden, The Netherlands*

[2]*Genexpress, Leiden Institute of Chemistry, P.O. Box 9502 2300 RA Leiden, The Netherlands*

**Corresponding author*

Empty capsids (artificial top component) of turnip yellow mosaic virus were co-crystallized with an encapsidation initiator RNA hairpin. No clear density was observed for the RNA, but there were clear differences in the conformation of a loop of the coat protein at the opening of the pentameric capsomer (formed by five A-subunits) protruding from the capsid, compared to the corresponding loop in the intact virus. Further differences were found at the N terminus of the A-subunit. These differences have implications for the mechanism of decapsidation of the virus, required for infection.



*Keywords:* artificial top component; TYMV; X-ray crystallography

## Introduction

Turnip yellow mosaic virus (TYMV) is a non-enveloped plant RNA virus and is the type member of the genus *Tymovirus*. The virion is an icosahedral particle with $T=3$ symmetry and the protein shell consists of 180 identical subunits. The viral capsid is stabilized mainly by protein–protein interactions,[1] hence the ability of the virus to produce empty capsids (natural top component, NTC).[2] Viral RNA can be separated from the intact virus by various methods, leaving the protein shell largely intact, such as incubation in the presence of a high concentration of urea or formamide, alkaline treatment, heating or freezing and thawing.[1] Over the past years TYMV, NTC and artificially obtained empty capsids (artificial top component, ATC) have been studied extensively using many different techniques. Low-resolution diffraction studies have been performed on TYMV, ATC and NTC. From these studies it was concluded that the structures of these particles are most likely very similar.[3,4] In addition, TYMV and NTC could be co-crystallized indistinguishably,[2] with several cryo-electron microscopy studies (cryo-EM) corroborating the findings of a high level of similarity between the intact virus and empty particles.[2,5–8] Furthermore, from cryo-EM studies in combination with analytical ultracentrifugation, X-ray scattering and X-ray diffraction and orientation in a magnetic field, it was concluded that the RNA leaves the virus *via* a hole in the capsid left by the dissociation of at least one pentameric capsomer, whereas the rest of the capsid remains intact.[9] A high-resolution structure of TYMV has been reported by Canady *et al.*[10] To date, however, no high-resolution structure of the empty capsids of TYMV is available. For another virus belonging to the genus *Tymovirus*, both the structure of the intact virus and its empty capsid are available.[11,12] Comparison of the two structures proved helpful in providing indirect evidence for protein–RNA interactions as parts of the N termini of the A, B and C subunits were visible in the presence of viral RNA, whereas in the absence of RNA they were disordered.

Presently, not much is known about protein–RNA interactions in TYMV. The organization of RNA in TYMV was studied using small-angle neutron-scattering.[13] Results indicated that the RNA is organized within the interior of the protein capsid with little or no penetration into the coat protein. On the other hand, crosslinking studies have demonstrated that interactions should occur between RNA and protein.[14] However, the X-ray structure of TYMV could not provide direct evidence to corroborate these findings.[10] No clear electron density in the vicinity of the coat protein was found that could be ascribed to RNA. However,

Present address: H. H. J. Bink, De Ruiter Seeds C.V., P.O. Box 1050, 2660 BB Bergschenhoek, The Netherlands.

Abbreviations used: TYMV, turnip yellow mosaic virus; NTC, natural top component; ATC, artificial top component; cryo-EM, cryo-electron microscopy; HP, hairpin; UTR, untranslated region.

E-mail address of the corresponding author: raj@chem.leidenuniv.nl

strong density organized around the 5-fold axis in the interior of the virus capsid was found but with no apparent interactions with the coat protein. On the contrary, in a cryo-EM study, ordered regions of RNA were found touching the coat protein at the 3-fold axis rather than at the 5-fold axis.[7] Furthermore, from *in vitro* binding assays and gel mobility-shift electrophoresis, it was concluded that a 5′-proximal hairpin (HP1) of TYMV RNA binds specifically to the interior of an empty TYMV capsid under slightly acidic conditions and in the presence of spermidine, whereas no interaction was observed under neutral conditions.[15] In TYMV, as well as in other members of the genus *Tymovirus*, the 5′ untranslated region (UTR) of the genomic RNA was shown to contain hairpins with internal loops consisting solely of C·C and C·A oppositions.[16] Extensive studies revealed that the conserved C·C and C·A pairs in the stem-loop structure are of major importance for its function in encapsidation initiation.[17] It was postulated that under acidic conditions protonation of cytosine and adenine bases occurs, thereby forming $C^+$·C and $A^+$·C base-pairs. These $C^+$·C and/or $A^+$·C pairs may share a proton with carboxylic side-chains of acidic amino acids, which then would represent a novel type of RNA–protein interaction.[15] Recently, it has been suggested that the whole TYMV viral RNA genome can form 20–30 hairpins, containing the $C^+$·C and $A^+$·C base-pairs. The protonation and deprotonation of these C·C and A·C base-pairs is proposed to be a driving force for encapsidation and disassembly of the TYMV virion (H.H.J.B. *et al.*, unpublished results).

Previously, a study was performed on bacteriophage MS2 that was soaked with an RNA hairpin, which is thought to play a role in assembly of the phage capsid.[18] The X-ray structure showed binding of specific RNA bases of the hairpin to conserved residues of the coat protein. Later, in a cryo-EM study, the interaction of viral RNA with the MS2 coat protein was visualized, confirming that the binding of the hairpin was not just an artifact of the crystallization.[19] In analogy with these studies, we co-crystallized the 5′-proximal hairpin HP1 with ATC and solved the structure of this capsid complex. Although no density was observed for the RNA hairpin, differences were observed between the intact TYMV particles and the ATC capsids, which may provide further clues in the elucidation of the nature of the interaction between viral RNA and the protein capsid.

## Results

### Data collection and structure of empty capsids of TYMV

Most X-ray data from virus crystals are obtained at room temperature as it is often difficult to find suitable freezing conditions. However, freezing reduces the radiation-induced decay and allows a complete dataset to be measured from a single crystal. ATC crystallizes in the presence of high salt (1.2 M ammonium phosphate). Therefore, we investigated freezing conditions with cryosalts rather than with the more traditional organic cryoprotectants, such as glycerol.[20] Several different saturated solutions of salts in various ratios with 1.2 M ammonium phosphate (pH 4.5) were tested (Table 1). These salts had to be compatible with the high concentration of phosphate already present in the solution and should not affect the pH of the solution, which is important for the eventual binding of the RNA hairpin to the capsid protein. Crystals frozen in a 4:1 (v/v) lithium sulfate/ammonium phosphate solution gave the best diffraction images.

A complete dataset was measured from one ATC crystal and the structure of these empty capsids of turnip yellow mosaic virus was solved to 3.75 Å resolution. The crystals belong to spacegroup $F4_132$, with cell dimensions of 688.5 Å. This spacegroup and cell dimensions were reported for crystals grown from 0.7 M ammonium sulfate.[3] A summary of the refinement statistics is given in Table 2. The rather high $R_{merge}$ is caused by the weakness of the data, yet, because of the high multiplicity, acceptable values for $I/\sigma$ could be obtained.

The structure was solved by molecular replacement using the structure of the intact virus (PDB accession code 1AUY)[10] after establishing that the asymmetric unit contains five of the three icosahedrally independent subunits designated A, B and C (Figure 1), which are chemically identical (following the nomenclature used by Harrison *et al.*)[21] due to the symmetry imposed by the spacegroup. The unit cell contains eight virus particles, with a lattice of a diamond type. The structure was refined to a final *R*-factor of 24.5% ($R_{free}$ 25.1%). The overall structure is of good quality, with 98.5% of the residues lying in the most favored and additionally allowed regions in the Ramachandran plot.[22] The RMSD in bond distances is 0.008 Å and the RMSD in bond angles is 1.50° from the Engh & Huber values.[23] The overall structure of the A, B and C subunits is very similar (Figure 1), having a topology found in virtually all spherical plant

**Table 1.** Cryosalt saturated solutions used to test for suitable freezing conditions for ATC crystals

| Cryoprotectant | Ratio[a] | Freezing[b] |
|---|---|---|
| Lithium fluoride | 9:1 | Clear |
| Lithium fluoride | 4:1 | Clear |
| Lithium fluoride | 1:1 | Precipitate |
| Ammonium fluoride | 3:2 | Clear |
| Sodium chloride | 1:1 | Precipitate |
| Lithium sulfate | 9:1 | Clear |
| Lithium sulfate | 4:1 | Clear |
| Lithium sulfate | 1:1 | Precipitate |

[a] Ratio (v/v) of cryosalt saturated solution with 1.2 M ammonium phosphate (pH 4.5).
[b] The frozen drops were inspected visually to see if they were clear and one diffraction image was taken to check for ice-rings.

**Table 2.** Data collection and refinement statistics

| | ATC |
|---|---|
| *Data collection* | |
| Beamline | ESRF ID29 |
| Wavelength (Å) | 0.98 |
| Resolution[a] (Å) | 25–3.75 (3.98–3.75) |
| Completeness (%) | 100 (99.3) |
| Measured reflections | 1,267,930 |
| Unique reflections | 141,239 |
| $R_{merge}$[b] (%) | 20.4 (59.5) |
| Average $I/\sigma$ ($I$) | 10.7 (2.7) |
| *Refinement* | |
| $R$-factor (%) | 24.5 (28.6) |
| Free $R$-factor (%) | 25.1 (28.4) |
| No particles in unit cell | 8 |
| No atoms in asymmetric unit | 20470 |
| Average total $B$-value (Å$^2$) | 44.0 |
| *Validation* | |
| Ramachandran plot (%) | |
| Most favored region | 71.3 |
| Additionally allowed region | 27.2 |
| Generously allowed region | 0.7 |
| Disallowed region | 1.1 |
| RMSD values | |
| Bond lengths (Å) | 0.008 |
| Bond angles (deg.) | 1.5 |

[a] Values of reflections recorded in the highest-resolution shell are shown in parentheses.
[b] $R_{merge} = \Sigma(|I - \langle I \rangle|)/\Sigma(I)$ (scalepack output).

viruses, the beta-barrel motif. As in other $T=3$ virus structures, the A-subunits form the pentamers around the icosahedral 5-fold axis, the B and C subunits together form the hexamers, and are related by quasi 6-fold symmetry (Figure 2). The subunits A, B and C are related by quasi 3-fold symmetry. The pentamers and hexamers protrude from the surface, leaving a deep depression at the quasi 3-fold axis surrounded by the A, B and C subunits.

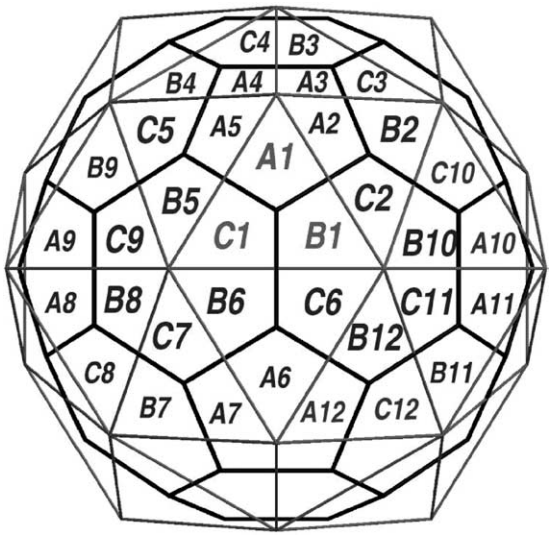


**Figure 2.** A representation of $T=3$ viral architecture. The picture was taken from the VIPER website.[25]

## Electron density map

After the molecular replacement solution was obtained, several rigid body refinements and grouped $B$-factor refinement cycles were performed using strict non-crystallographic symmetry and electron density maps were calculated. These maps were of such good quality that there was no need for real space averaging over the 5-fold non-crystallographic symmetry of the asymmetric unit. We attempted to co-crystallize the ATCs with an RNA encapsidation initiation hairpin HP1 by growing crystals of the ATC in the presence of an

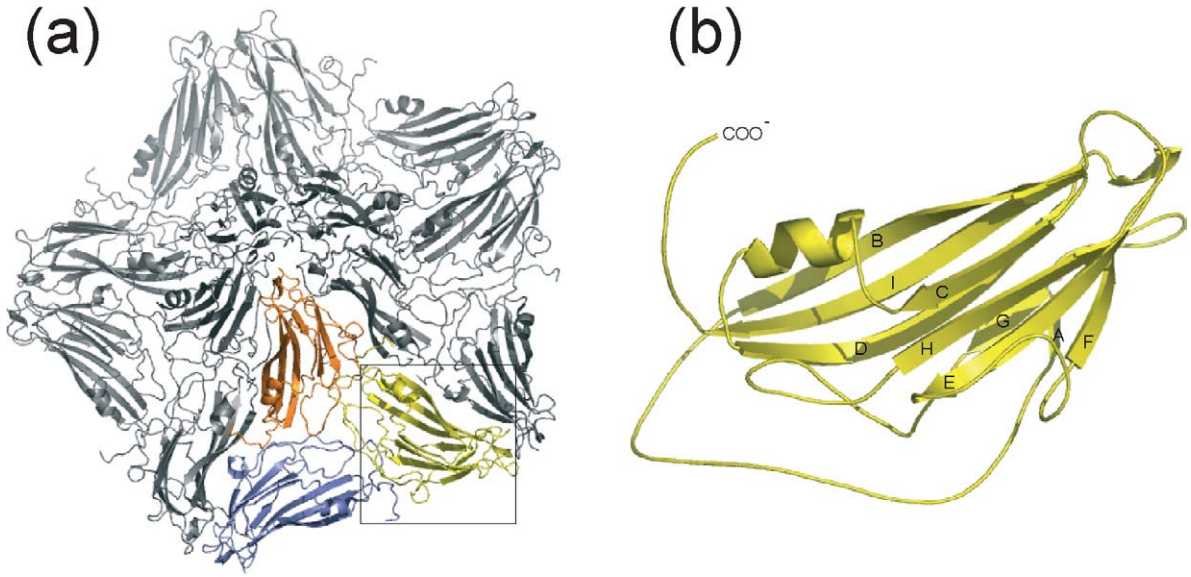


**Figure 1.** (a) Pentamer of subunits A (orange), B (yellow) and C (blue) present in the asymmetric unit. (b) Secondary structure of the subunits, the beta-strands of the jellyroll beta-barrel are labeled. The nomenclature for the BIDG and CHEF strands follows that used by Harrison *et al.*[21] The picture was created using PyMol Molecular Graphics System (http://www.pymol.org).

RNA initiator hairpin at pH 4.5, as it has been shown that this is the pH optimum for binding of the RNA hairpin to the coat protein.[15] Binding of RNA to the coat protein under the conditions used for crystallization has never been shown, as these conditions are unsuitable for performing the standard binding assay (based on a shift in electrophoretic mobility), due to the high concentration of salt. However, the integrity of the RNA hairpin during co-crystallization was analyzed and after two months of crystallization at room temperature under various salt conditions the hairpin was still intact in the crystallization drops (Figure 3).

No clear electron density was observed for the RNA hairpin. Some extra electron density was found in the vicinity of two histidine residues, H68 and H180 (Figure 4), which are accompanied by residues R67, R140 and D143. These residues are located in a cavity surrounded by R12-E135 and K32-E72 (Figure 5). All these residues are located at the interior surface of the capsid close to the interface between subunits A, B and C at the bottom of the depression. Previously, these residues were implicated to play a role in RNA binding.[10,14,24] The RNA hairpin does not likely coincide with the viral symmetry, hence its electron density would not be seen. Modeling ions such as phosphate or magnesium into this difference density as an alternative for RNA was not successful. Additional extra density was also present along beta-strand G of subunit A, which could be ascribed to part of the N-terminal region of the A-subunit (data not shown). By overlaying subunit B onto A, part of the N terminus of the B-subunit approaches this density. As a result, amino acid residues 10–15 of the A subunit could be built into the density and refined. This loop is rather flexible, as shown by the high average *B*-factor for this region.

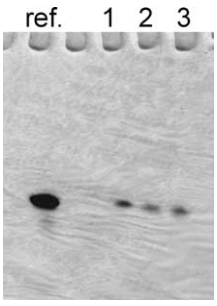


**Figure 3.** The integrity of the RNA HP1 during co-crystallisation. RNA from crystallization droplets with various concentrations of salt was analyzed by 10% polyacrylamide gel electrophoresis under denaturing conditions (8 M urea), after two months of crystallization at room temperature. Lane 1, 1.18 M ammonium phosphate. Lane 2, 1.22 M ammonium phosphate. Lane 3, 1.24 M ammonium phosphate. In the lane with the reference, intact RNA HP1 was loaded. The gel was stained with toluidine blue.

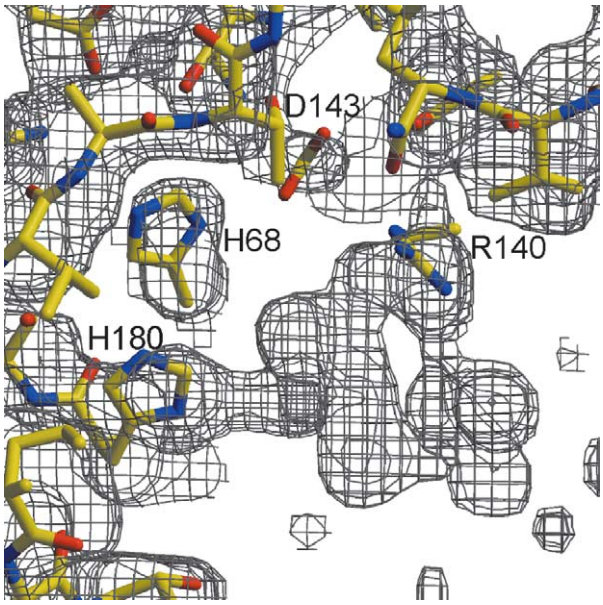


**Figure 4.** $2F_o - F_c$ electron density map contoured at 1σ. Extra electron density, perhaps of the poorly ordered RNA hairpin, is observed in a cavity formed by H68 and H180, R67, R140 and D143. In this orientation, R67 lies exactly behind H68 and can therefore not be observed in this picture. The picture was created with Xtalview.[34]

## Comparison with TYMV

We have crystallized the ATC using crystallization conditions similar to those used for the intact virus and, to our surprise, ATC crystallized in a different

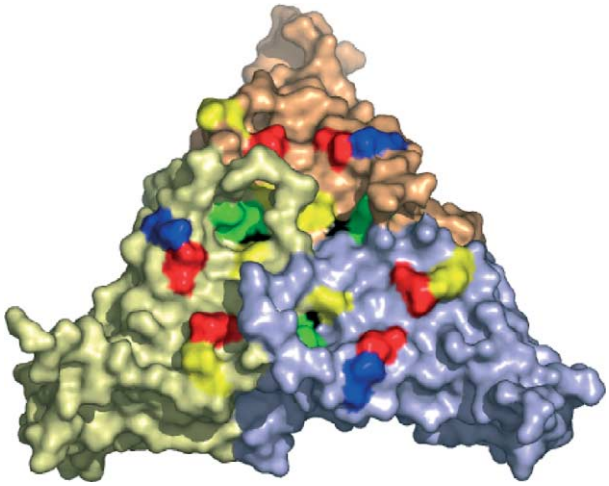

**Figure 5.** Surface representation of subunits A (orange), B (yellow) and C (blue) viewed along the quasi 3-fold axis from the interior of the capsid. The histidine 68 and histidine 180 (green) are located close to the interface between subunits A, B and C. The cavities containing histidine 68 and histidine 180 (green), accompanied by Arg67, Arg140 (yellow) and Asp143 (black) are surrounded by a Arg-Glu and a Lys-Glu couple (R12/E135 and K32/E72) (yellow/red and blue/red, respectively). The side-chain of these residues point towards the interior of the capsid.

**Table 3.** Comparison of TYMV and ATC crystals

| | TYMV[a] | ATC |
|---|---|---|
| Crystallization conditions | 1.11–1.15 M ammonium phosphate, 100 mM Mes, pH 3.7 | 1.16 M ammonium phosphate, pH 4.5 |
| Spacegroup | $P6_422$ | $F4_132$ |
| Unit cell parameters | $a=b=515.5$ Å, $c=309.4$ Å, $\alpha=\beta=90°$, $\gamma=120°$ | $a=b=c=688.5$ Å, $\alpha=\beta=\gamma=90°$ |

[a] Crystallization data were obtained from Canady *et al.*[26]

spacegroup ($F4_132$ rather than $P6_422$, Table 3). In the empty particles, crystal contacts between the particles occur at the quasi 6-fold positions only. At the top of the hexamer, a loop from residue 161 to 165 "kisses" the same loop in a neighboring particle. In the intact virus, however, a more efficient packing exists (Figure 6). An ATC particle occupies up to 1.5 times more space in the unit cell than the intact virus particles. Both pentamers and hexamers are involved in the packing for TYMV. A pentamer from one particle snuggles up into the depression in between the pentamer and the hexamer, making numerous contacts *via* the beta-strands of the protruding pentamers and hexamers. In order to release genomic RNA from the intact virus particles by freezing and thawing, it has been suggested that the particles must lose a pentamer.[9,7] Although this hole cannot be observed by X-ray crystallography, as it gets averaged out due to the random orientations of the particles in the crystal, it could be the reason that the empty particles pack only at the hexamers and not at the pentamers. These observations may explain the reduction in crystalline order in the ATC crystals (diffracting to 3.75 Å)

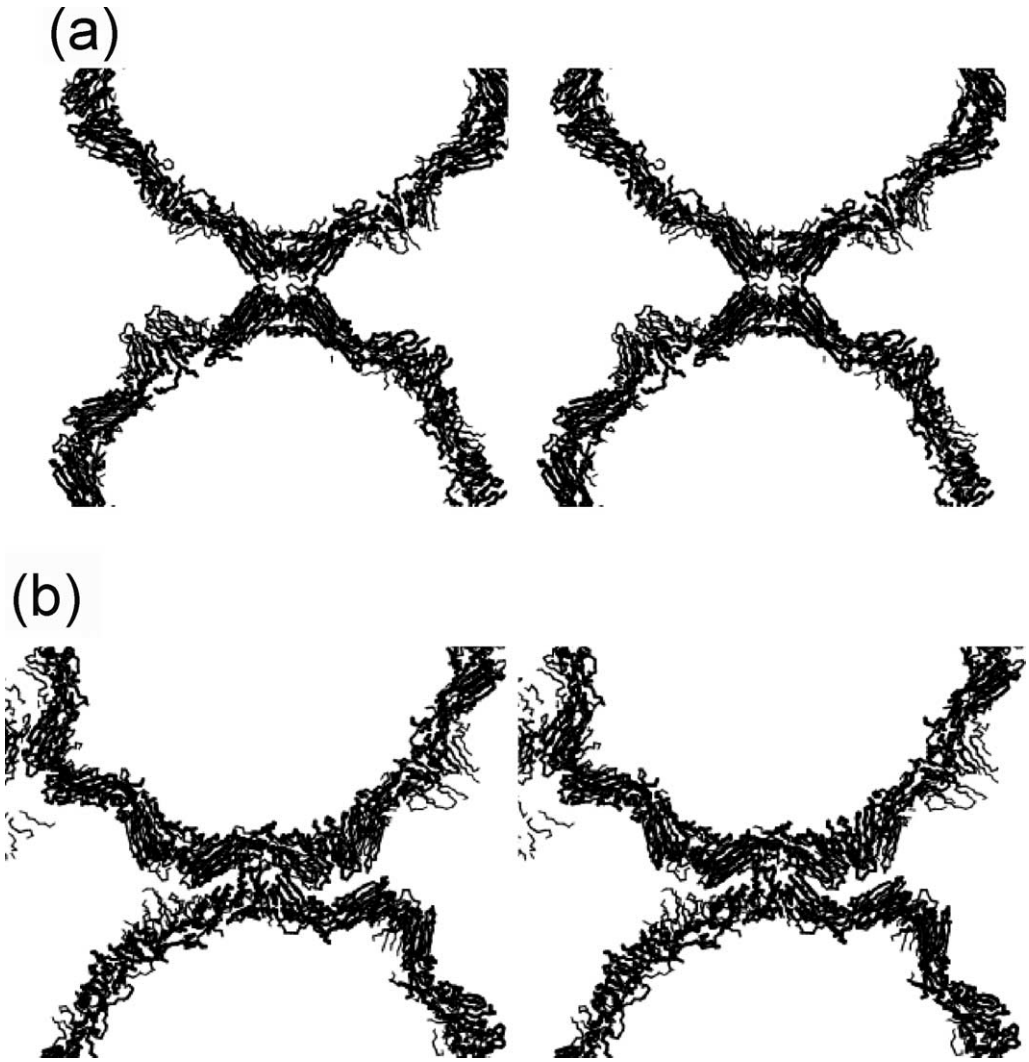


**Figure 6.** Crystal packing of (a) ATC and (b) TYMV. A difference in packing can be observed immediately. ATC interacts *via* tips of the hexamers, whereas in TYMV a pentamer protrudes into the depression formed by A, B and C at the quasi 3-fold axis. The difference in packing may be explained by the loss of a single capsid pentamer in the ATC.

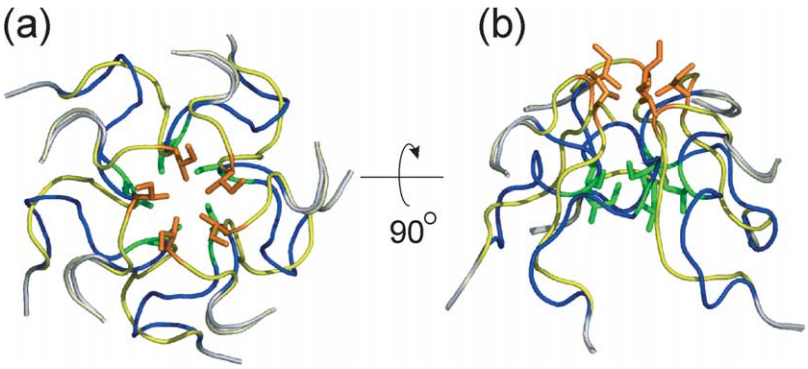


**Figure 7.** (a) Top view along the 5-fold axis of an overlay of a loop containing residues 117 to 135 of subunit A from ATC (yellow) and TYMV (blue), with the loops containing G120 to L128 highlighted. (b) A 90° rotated side view of the overlay. The side-chain of I122 is shown in both models, orange in ATC and green in TYMV. From this picture it becomes clear that this loop in ATC has flipped in an upward direction, changing the opening of the pentamer.

compared to crystals of the intact virus (diffracting to 3.2 Å).

In contrast to the general similarity of the capsid structures of ATC and TYMV, a major difference was found in a loop of subunit A at the opening in a depression of the pentamer (Figure 7). The residues in this loop in both the TYMV and the ATC structures have high *B*-factors, suggesting that this loop is very flexible. Despite this, difference density did clearly indicate a different conformation of the loop in ATC rather than disorder. The loop starts at amino acid residue G120 running to L128 in the A subunit. Significantly, this loop with I122 at the tip is pointing towards the interior of the pentamer in TYMV, while in ATC this loop rotated about 90° towards the top of the pentamer; I122 is now pointing outwards, leaving a smaller opening in the depression of the pentamer. The distance between opposite side-chains of the ILe is about 3.5 Å, whereas in TYMV the distance between the side-chains of this ILe is approximately 4.8 Å. Because of the large conformational change in this loop, the opening at the depression of the pentamer lies approximately 9 Å deeper in TYMV than in ATC. The fact that both structures have high non-crystallographic symmetry of trimers, formed by subunits A, B and C, 5-fold in the case of ATC and 15-fold in the case of TYMV, suggests that the differences observed between the loops are not likely due to crystal packing.

Earlier biochemical and cryo-EM studies had established that the diameter of the full and empty particles is similar.[6,7] When pentamers or hexamers lying on exactly opposite sites in the capsids of ATC are overlaid on top of the TYMV capsid, the diameter is 2.1 Å shorter for the pentamer and 1.5 Å shorter for the hexamers. At a resolution of 3.75 Å these are small, but significant differences, which could not have been observed from cryo-EM studies.

Finally, the association energies and the buried surface areas between the subunits have been calculated using the virus particle explorer (VIPER, Figure 2, Table 4).[25] The data for TYMV were available from the VIPER website†. As expected for very similar structures, no major difference was found. Except for the increase of buried surface area and association energy between subunits at the icosahedral 5-fold and at the quasi 3-fold axis between subunit A and B, which can be explained by the presence of part of the N terminus of the A subunit in ATC. This N terminus, which is not modeled in the TYMV structure, interacts with the A2 and B subunits and hence increases the association energy and the buried surface area. Furthermore, the influence of the conformational change in the loop at the opening in the apex at the icosahedral 5-fold axis was checked. The surface area and the association energy of ATC were recalculated with residues 10 to 15 of the A subunit left out of the model. Similar values were found as for TYMV (data not shown), showing that this conformational change in the loop of subunit A does not have an effect on the stability of the capsomer.

† http://mmtsb.scripps.edu/viper/

## Discussion

Crystals of TYMV grown from 1.11–1.15 M ammonium phosphate at pH 3.7 (Table 3) belong to the hexagonal spacegroup $P6_422$,[26] whereas crystals of ATC, described here, grown from 1.16 M ammonium phosphate at pH 4.5 belong to the cubic spacegroup $F4_132$. Interestingly, Klug *et al.*[3] found that both TYMV and ATC crystallize in the cubic spacegroup with similar cell dimensions, using 0.7 M ammonium sulfate. Therefore, the presence of a hole of at least one pentamer in the ATC capsids *versus* its absence from the intact virus may not be sufficient to explain this difference. Perhaps the binding of RNA to the coat protein induced this difference. TYMV was grown in ammonium phosphate at pH 3.7 by Canady *et al.*,[26] whereas the crystals obtained by Klug *et al.*[3] were most likely grown at a higher pH, as the pH of 0.7 M ammonium sulfate solution is around 5.5, which might have an influence on RNA binding. No viral RNA is present in our structure. The major difference found between TYMV and ATC is located in a loop from amino acid residues G120 to L128 in the A subunits, which is located at the opening within a pentamer. It has been suggested that the viral RNA leaves the virus

**Table 4.** Comparison of association energies and buried surface area between subunits around symmetry axes in ATC and TYMV

| Subunit interface | Quasi/icosahedral symmetry | Association energies (kcal mol$^{-1}$) | | Buried surface area (Å$^2$) | |
|---|---|---|---|---|---|
| | | ATC | TYMV | ATC | TYMV |
| A1-A2 | Icos. 5-fold | −40 | −33 | 2075 | 1794 |
| A1-B1 | Quasi 3-fold | −34 | −25 | 1751 | 1410 |
| A2-B1 | Quasi 2-fold | −30 | −31 | 1676 | 1755 |
| A1-C1 | Quasi 3-fold | −33 | −32 | 1728 | 1700 |
| B1-C1 | Quasi 3-fold | −44 | −44 | 2196 | 2217 |
| B1-C2 | Quasi 6-fold | −48 | −50 | 2461 | 2604 |
| B1-C6 | Quasi 6-fold | −50 | −49 | 2495 | 2531 |
| C1-C6 | Icos. 2-fold | −32 | −32 | 1779 | 1812 |

particles *via* a hole in the capsid, generated by the loss of at least one pentamer. Perhaps subunit A undergoes some structural rearrangement to facilitate the loss of a pentamer, which is reflected in the differences between the A subunit of ATC compared to that of TYMV. Most likely, the changes in these loops are not caused by crystal packing interactions, since both structures have a high degree of non-crystallographic symmetry and the multiple copies of the trimers present in the asymmetric unit have different surroundings. Thus, the different loop conformations appear to be a biological feature of the viral capsids.

It would not be surprising that some interaction occurs between the viral RNA and the A-subunits. It was suggested that a unique RNA sequence will interact with a particular group of residues from the protein capsid.[9] Furthermore, binding studies between the viral coat protein and the RNA hairpin HP1, located at the 5′ terminus of the genomic RNA have shown that the interaction occurs only at low pH.[15] Although the loop in the A-subunit that changes its conformation does not contain any residue that might interact with RNA directly, the conformational change might be caused by interaction with the N terminus of the A-subunit, which we show here to have a different conformation compared to the intact virus. Contrary to what was found in the higher-resolution TYMV structure, in the ATC structure we did observe part of the N terminus of the A-subunit. This may suggest that the N terminus of subunit A in TYMV interacts in a non-unique way with the TYMV genomic RNA. The electron density maps of TYMV showed, in agreement with earlier cryo-EM studies, regions of ordered RNA within the particles at a radius of 90 Å, although no direct interaction with the coat protein was observed. However, along the 5-fold axis pronounced projections of RNA extending to approximately 75 Å were observed.[10] Perhaps some RNA interacts with the coat protein, but not according to the crystallographic and icosahedral symmetry, which would explain why it is not visible in the electron density maps of the intact TYMV. We propose that in the absence of viral RNA the N terminus of the A subunit, which is very flexible, undergoes structural rearrangements and then interacts with the beta-strand G in ATC, thereby becoming partially visible in the symmetrized structure. From RNA crosslinking studies at pH 4.8 it is clear that, along with two other regions, the N terminus is involved in binding the RNA.[14] Similar UV crosslinking studies at pH 7.3 did not introduce any crosslinks, indicating that the RNA does not interact with the coat protein at this higher pH.

Another region (residues 132–152) indicated by Ehresmann *et al.*[14] to crosslink with RNA is located close to the N terminus and in the TYMV structure extra density around these residues was observed. Moreover, two histidine residues, 68 and 180, which are exposed at the interior of the virus capsid are located very close to both the N terminus and residues 132–152 and had been suggested as potential candidates for interaction with the RNA.[10] Mutagenesis of these histidine residues to alanine has a strong effect on virus transport in the infected plant, which supports a role for these residues in RNA encapsidation.[24] It may be the case that RNA discriminates between the chemically identical subunits A, B and C because of the difference in the size of the apex of the pentamer compared to the hexamer, which are formed by the A or the B and C subunits respectively. As the N termini of the B and C subunits are involved in stabilization of the hexamers, they would not be available to engage in RNA binding.

Despite the differences in crystal packing and in the loop of subunit A, the overall structures of TYMV and ATC are very similar. This confirms that the capsid is stabilized mainly by protein–protein interactions and not protein–RNA interactions.[1] From very early X-ray diffraction studies,[3] structural similarity between TYMV, NTC and ATC was already established. Moreover, the same results have been obtained by cryo-EM studies.[5–7]

In the TYMV structure extra density was observed around residues H68, H180, R67 and R140. Therefore, it is not unreasonable to expect the RNA initiator hairpin HP1 to bind in this area. In the ATC containing a short RNA hairpin, extra density was observed in this region (Figure 4). However, it was not possible to ascribe this extra density to any particular nucleic acid moiety. Most likely, the RNA hairpin does not obey the icosahedral symmetry present within the virus particles,

averaging out its electron density. The observed extra density might be the result of alignment of part of the hairpin at this position within the capsid and therefore visible, whereas the rest of the hairpin is out-of-register with the symmetry. Furthermore, because of the high level of symmetry present within the virus capsid, the hairpin may be distributed equally among the five or six equivalent positions in a capsomer. The latter may seriously hamper a successful elucidation of the RNA–protein interactions in TYMV. Yet, there is a possibility that under the crystallization conditions used, this hairpin did not fully bind to the coat protein. Therefore, new crystallization conditions will be explored, which are more suitable for binding of the hairpin to the coat protein.

In conclusion, the structure of the coat protein of TYMV is affected by the presence or the absence of genomic RNA inside the virus. No interaction was observed between the coat protein and an RNA hairpin that contains the proposed capsid recognition motif. Further studies will be required to establish whether there are conditions in which this interaction becomes sufficiently ordered to be visualized by X-ray diffraction techniques. A clearly different conformation was found for a loop in the A subunit located at the opening of the pentamer, and part of the N terminus of the A subunit is visible in the ATC structure. These differences may confirm evidence for interactions between the coat protein and viral RNA at the N terminus at the icosahedral 5-fold axis, depending on the pH and the state of the virus. We propose that this RNA–protein interaction plays a role in encapsidation or decapsidation of the virus, as it has been described that the virus on decapsidation loses at least one pentamer through which the viral RNA can escape.

## Materials and Methods

### Production and purification of empty capsids

TYMV was isolated from infected leaves of Chinese cabbage (*Brassica pekinensis*) plants three weeks after inoculation. Inoculation of the plants was performed with *in vitro* transcribed and capped genomic TYMV RNA. The infectious cDNA clone of the Blue Lake strain of TYMV, pBL16,[27] was used as template. Conditions of plant growth and inoculation were as described.[15] Isolation of TYMV from the infected leaves was done using the bentonite procedure, as described.[28] On average, 40 infected plants provide 350–400 g of infected leaf material after the major vein material was discarded. The virus preparation obtained after the various centrifugation steps was resuspended in 10 mM Tris–HCl (pH 7.0) with a final concentration of 80–90 mg $ml^{-1}$. The virus yield is about 1 mg per g of infected leaf material.

Artificial top component (ATC) was prepared from TYMV virions using the freeze–thaw method as described.[8] Aliquots of 0.4 ml of virus suspension in 30 mM sodium acetate (pH 7.0) and a concentration of 8 mg $ml^{-1}$ were frozen in liquid $N_2$ for two minutes and thawed at room temperature. The aliquots were pooled and supplemented with cesium chloride (1.90 g $ml^{-1}$) and 10 mM sodium acetate buffer (pH 6.0). Before centrifugation, the initial density of the cesium chloride mixture was 1.26 g $ml^{-1}$. Centrifugation was done for 16 hours at 60,000 rpm at 10 °C in a Beckman NVT-65 rotor. Two layers of protein formed; and the upper layer was taken for further processing. The second layer contains primarily NTC complexed with cesium, as described.[29] Genomic RNA and undegraded B-component (filled virions) were present at the bottom of the tube. The samples were dialyzed for 24 hours against 10 mM sodium acetate (pH 6.0) at 4 °C with regular buffer exchanges (with 2 l, at least five times). The dialyzed ATC suspension was filtered over a 0.24 μm pore size filter (Schleicher and Schuell). Finally, ATC was pelleted (60 minutes at 45,000 rpm at 4 °C in a Beckman 75 Ti-rotor) and resuspended in 10 mM sodium acetate (pH 6.0; final concentration 15 mg $ml^{-1}$). The quality of the ATC preparation was analyzed using agarose gel electrophoresis and *in vitro* binding assays (data not shown).

The RNA fragment corresponding to the TYMV encapsidation initiation hairpin HP1 (5′ CCAGC UCUCU UUUGA CAACU GG 3′) was synthesized chemically as described.[15]

### Crystallization

Before crystallization, the sample was filtered through a low protein-binding 0.22 μm pore size filter (Millipore). Crystals of ATC were grown in 1.16–1.22 M ammonium phosphate (pH 4.5) at room temperature, using the sitting-drop, vapor-diffusion method (as described for TYMV).[26] A large number of small crystals appeared within a few days from mixing 5 μl of protein solution with an equal volume of precipitant solution. Crystals of ATC with the RNA hairpin were obtained by crystallization with a protein to ligand molar ratio of 1:50. $MgCl_2$ (10 mM) was added to the precipitant solution to replace the spermidine, which is naturally present in TYMV.[30] Spermidine is subject to oxidation and therefore not suitable for this type of experiment. Furthermore, RNase inhibitor (RNA Guard, Pharmacia) was added in a 1:50 (v/v) dilution to the crystallization droplet to prevent the RNA oligonucleotide from degradation. Mixing equal volumes of protein solution, in the presence of 50 equivalents of RNA hairpin, with reservoir solution, again resulted in a large amount of rather small crystals, which were not suitable for X-ray crystallography. In order to grow larger crystals, the protein concentration was lowered to 10 mg $ml^{-1}$ and 5 μl of this protein solution was mixed with an equal volume of precipitant solution. After equilibration, macroseeds obtained from previous crystallization trials were washed in reservoir solution and transferred to the new crystallization droplets. In these drops, no spontaneous nucleation had occurred and the macroseeds grew into large crystals with dimensions up to 0.6 mm × 0.4 mm × 0.25 mm.

### Data collection and processing

X-ray diffraction data of the ATC crystals grown in the presence of the RNA fragment were measured at the protein X-ray crystallography beamline ID29 at the European Synchrotron Radiation Facility in Grenoble, France on an ADSC Q210 CCD detector. The crystals were soaked for a few seconds in a cryoprotectant solution containing saturated solution of lithium sulfate and 1.2 M ammonium phosphate (pH 4.5), mixed in a ratio 4:1 (v/v), and 0.45 mM RNA, followed by flash-freezing in a nitrogen gas stream at 100 K. Data were collected using

0.25° oscillations and 200 images were recorded per dataset. The collected data were indexed, integrated and scaled with HKL2000.[31] A summary of the processing statistics is given in Table 2.

### Structure determination and refinement

A complete data set was taken from one crystal at 100 K and the data were processed to 3.75 Å resolution. The structure was solved by molecular replacement using the structure of the intact TYMV (PDB accession code 1AUY)[10] as a search model in Molrep.[32] The molecular replacement solution had an *R*-value of 0.480 ($R_{free}$ 0.499) for data to 5 Å. The asymmetric unit contains a pentamer of A, B and C subunits. Several cycles of rigid body refinement, followed by alternating energy minimization and grouped temperature factor refinement runs, using strict 5-fold non-crystallographic symmetry (NCS) constraints in the CNS program,[33] the *R*-value dropped to 0.245 with an $R_{free}$ of 0.251 for data to 3.75 Å. Electron density maps were calculated and, where necessary, the model was rebuilt.

### Protein Data Bank accession code

The coordinates and structure factors have been deposited in the Protein Data Bank, under accession code 1W39.

## Acknowledgements

We thank Mr Nico Meeuwenoord for the synthesis of the RNA hairpin, and Dr Zbyszek Dauter and Dr Pierre Legrand for assistance in analyzing the diffraction images. Furthermore, we acknowledge the European Synchrotron Radiation Facility at Grenoble, France, for provision of facilities. We thank Dr Sean McSweeney for assistance in using beamline ID29, Dr RAG de Graaff for useful discussions and Ellen Thomassen for helping with the data collection.

## References

1. Kaper, J. M. (1975). The chemical basis of virus structure, dissociation and reassembly. In *Frontiers in Biology* (Neuberger, A. & Tatum E. L., eds), vol. 39, pp. 1–485, North-Holland, American Elsevier, Amsterdam, New York.
2. Markham, R. (1951). Physicochemical studies of the turnip yellow mosaic virus. *Discuss. Faraday Soc.* **11**, 221–227.
3. Klug, A., Longley, W. & Leberman, R. (1966). Arrangement of protein subunits and distribution of nucleic acid in turnip yellow mosaic virus. I. X-ray diffraction studies. *J. Mol. Biol.* **15**, 315–343.
4. Longley, W. & Leberman, R. (1966). Structural similarity of artificial and natural top components of turnip yellow mosaic virus. *J. Mol. Biol.* **19**, 223–225.
5. Finch, J. T. & Klug, A. (1966). Arrangement of protein subunits and the distribution of nucleic acid in turnip yellow mosaic virus. 2. Electron microscopic studies. *J. Mol. Biol.* **15**, 344–364.
6. Adrian, M., Timmins, P. A. & Witz, J. (1992). *In vitro* decapsidation of turnip yellow mosaic-virus investigated by cryoelectron microscopy—a model for the decapsidation of a small isometric virus. *J. Gen. Virol.* **73**, 2079–2083.
7. Bottcher, B. & Crowther, R. A. (1996). Difference imaging reveals ordered regions of RNA in turnip yellow mosaic virus. *Structure*, **4**, 387–394.
8. Katouzian-Safadi, M., Favre, A. & Haenni, A. L. (1980). Effect of freezing and thawing on the structure of turnip yellow mosaic virus. *Eur. J. Biochem.* **112**, 479–486.
9. Katouzian-Safadi, M., Berthetcolominas, C., Witz, J. & Kruse, J. (1983). Evidence for the presence of a hole in the capsid of turnip yellow mosaic-virus After RNA release by freezing and thawing—decapsidation of turnip yellow mosaic-virus *in vitro*. *Eur. J. Biochem.* **137**, 47–55.
10. Canady, M. A., Larson, S. B., Day, J. & McPherson, A. (1996). Crystal structure of turnip yellow mosaic virus. *Nature Struct. Biol.* **3**, 771–781.
11. Krishna, S., Hiremath, C. N., Munshi, S. K., Prahadeeswaran, D., Sastri, M., Savithri, H. S. *et al.* (1999). Three-dimensional structure of physalis mottle virus: implications for the viral assembly. *J. Mol. Biol.* **289**, 919–934.
12. Krishna, S. S., Sastri, M., Savithri, H. S. & Murthy, M. R. N. (2001). Structural studies on the empty capsids of Physalis mottle virus. *J. Mol. Biol.* **307**, 1035–1047.
13. Jacrot, B., Chauvin, C. & Witz, J. (1977). Comparative neutron small-angle scattering study of small spherical RNA viruses. *Nature*, **266**, 417–421.
14. Ehresmann, B., Briand, J. P., Reinbolt, J. & Witz, J. (1980). Identification of binding-sites of turnip yellow mosaic-virus protein and RNA by crosslinks induced *in situ*. *Eur. J. Biochem.* **108**, 123–129.
15. Bink, H. H. J., Hellendoorn, K., van der Meulen, J. & Pleij, C. W. A. (2002). Protonation of non-Watson–Crick base pairs and encapsidation of turnip yellow mosaic virus RNA. *Proc. Natl Acad. Sci. USA*, **99**, 13465–13470.
16. Hellendoorn, K., Michiels, P. J. A., Buitenhuis, R. & Pleij, C. W. A. (1996). Protonatable hairpins are conserved in the 5′-untranslated region of tymovirus RNAs. *Nucl. Acids Res.* **24**, 4910–4917.
17. Hellendoorn, K., Verlaan, P. W. G. & Pleij, C. W. A. (1997). A functional role for the conserved protonatable hairpins in the 5′ untranslated region of turnip yellow mosaic virus RNA. *J. Virol.* **71**, 8774–8779.
18. Valegård, K., Murray, J. B., Stockley, P. G., Stonehouse, N. J. & Liljas, L. (1994). Crystal-structure of a bacteriophage-RNA coat protein–operator complex. *Nature*, **371**, 623–626.
19. Koning, R., van den Worm, S., Plaisier, J. R., van Duin, J., Abrahams, J. P. & Koerten, H. (2003). Visualization by cryo-electron microscopy of genomic RNA that binds to the protein capsid inside bacteriophage MS2. *J. Mol. Biol.* **332**, 415–422.
20. Robinson, K. A., Ladner, J. E., Tordova, M. & Gilliland, G. L. (2000). Cryosalts: suppression of ice formation in macromolecular crystallography. *Acta Crystallog. sect. D*, **56**, 996–1001.
21. Harrison, S. C., Olson, A. J., Schutt, C. E., Winkler, F. K. & Bricogne, G. (1978). Tomato bushy stunt virus at 2.9 Å resolution. *Nature*, **276**, 368–373.
22. Ramachandran, G. N. & Sasisekharan, V. (1968). Conformation of polypeptides and proteins. *Advan. Protein Chem.* **23**, 283–438.

23. Engh, R. A. & Huber, R. (1991). Accurate bond and angle parameters for X-ray protein-structure refinement. *Acta Crystallog. sect. A*, **47**, 392–400.
24. Bink, H. H. J., Roepan, S. K. & Pleij, C. W. A. (2004). Two histidines of the coat protein of turnip yellow mosaic virus at the capsid interior are crucial for viability. *Proteins: Struct. Funct. Genet.* **55**, 236–244.
25. Reddy, V. S., Natarajan, P., Okerberg, B., Li, K., Damodaran, K. V., Morton, R. T. *et al*. (2001). Virus particle explorer (VIPER), a website for virus capsid structures and their computational analyses. *J. Virol.* **75**, 11943–11947.
26. Canady, M. A., Day, J. & McPherson, A. (1995). Preliminary-X-ray diffraction analysis of crystals of turnip yellow mosaic-virus (TYMV). *Proteins: Struct. Funct. Genet.* **21**, 78–81.
27. Skotnicki, M. L., Mackenzie, A. M. & Gibbs, A. J. (1992). Turnip yellow mosaic-virus variants produced from DNA clones encoding their genomes. *Arch. Virol.* **127**, 25–35.
28. Dunn, D. B. & Hitchborn, J. H. (1965). Use of bentonite in purification of plant viruses. *Virology*, **25**, 171–192.
29. Noort, A., Vandendries, C. L. A. M., Pleij, C. W. A., Jaspars, E. M. J. & Bosch, L. (1982). Properties of turnip yellow mosaic-virus in cesium-chloride solutions—the formation of high-density components. *Virology*, **120**, 412–421.
30. Beer, S. V. & Kosuge, T. (1970). Spermidine and spermine—polyamine components of turnip yellow mosaic virus. *Virology*, **40**, 930–938.
31. Otwinowski, Z. & Minor, W. (1997). Processing of X-ray diffraction data collected in oscillation mode. *Methods Enzymol.* **276**, 307–326.
32. Vagin, A. & Teplyakov, A. (1997). MOLREP: an automated program for molecular replacement. *J. Appl. Crystallog.* **30**, 1022–1025.
33. Brünger, A. T., Adams, P. D., Clore, G. M., Delano, W. L., Gros, P., Grosse-Kunstleve, R. W. *et al*. (1998). Crystallography & NMR system: a new software suite for macromolecular structure determination. *Acta Crystallog. sect. D*, **54**, 905–921.
34. McRee, D. E. (1999). XtalView Xfit—a versatile program for manipulating atomic coordinates and electron density. *J. Struct. Biol.* **125**, 156–165.

***Edited by Sir A. Klug***

*(Received 25 May 2004; received in revised form 24 June 2004; accepted 30 June 2004)*